Solid Freeform Fabrication 2024: Proceedings of the 35th Annual International Solid Freeform Fabrication Symposium – An Additive Manufacturing Conference
Reviewed Paper

INTERLAYER FRACTURE OF LARGE AREA ADDITIVE MANUFACTURED SHORT FIBER COMPOSITES

Arief Yudhanto[a,*], Neshat Sayah[a], Douglas E. Smith[a]

[a]*Department of Mechanical Engineering, Baylor University, Waco, TX 76798, USA*

Abstract

This paper proposes an efficient experimental method to measure the mode I fracture toughness of large-area additive manufactured polymeric composites. By utilizing either single-bead or double-bead systems bonded to the double cantilever beam (DCB) configuration, we measure intrabead and interbead fracture toughness of acrylonitrile butadiene styrene (ABS) and short carbon fiber-reinforced ABS. The effect of rigid doublers (which are used to eliminate a premature compressive failure) is excluded in the calculation of total energy dissipation, producing a purely interlayer fracture toughness. We found that the critical fracture toughness of carbon fiber/ABS is lower than that of ABS due to the voids within and between the beads. The experimental and data reduction methods developed here can be utilized to optimize the interlayer adhesion of large-scale 3D printed materials.

Keywords: Fracture, short fiber composites, energy release rate, mode I fracture, voids

Introduction

The large-area extrusion/deposition technology enables the manufacturing of meter-scale solid polymeric structures constructed from relatively wide beads (6–10 mm) [1]. The mechanical integrity of such a large structure depends on the individual bead (intrabead) characteristics and the interlayer connection between beads (interbead). One of the inevitable characteristics is the void development during the extrusion process. In a large-area additive manufacturing (AM) of short carbon-filled acrylonitrile butadiene styrene (CF/ABS), for instance, the formation of voids within the bead is driven by the limited pressure on the surface around the fiber tip [2, 3]. In addition, voids that are formed between beads may act as a crack initiator and propagation path, producing low intrabead and interbead fracture properties.

*Corresponding author
Email address: arief_yudhanto@baylor.edu (Arief Yudhanto)

The fracture properties of AM polymers and composites have been measured experimentally by several authors [4–6], which have been shown to provide a good understanding of the fracture behavior of AM parts that enables the structural design based on damage tolerance criteria. For example, the fracture toughness (i.e., energy required by the cracked material to initiate a fracture) of 3D printed unfilled/neat ABS, as measured using single edge-notch specimens under tension (SENT), was found to be 0.24–0.88 kJ/m^2 [4] with a noticeable degree of orthotropy due to the raster orientation. Hart and Wetzel [5] found that the fracture of 3D-printed neat ABS also exhibited an orthotropy response where the measured fracture toughness was 0.25 kJ/m^2 for inter-laminar and 2.26 kJ/m^2 for cross-laminar. A higher print speed of 70 mm/s improved the fracture toughness of 3D-printed ABS with measured values up to 4.1 kJ/m^2 [6]. As a reference, the fracture toughness of the injection-molded ABS typically ranges between 1.37 and 6.00 kJ/m^2 [7–10], showing that the interlayer fracture toughness of 3D-printed neat ABS falls within the bounds of the injection molded samples.

Reinforcing bulk polymers by adding short fibers and varying processing conditions have been done to modify the fracture toughness of 3D-printed polymers. Barocio et al. [11] suggested that the fracture toughness of CF/PPS (a semi-crystalline polymer composite) is sensitive to the build plate temperature. By keeping the dwell time at 10 min, the fracture toughness of CF/PPS printed with the build plate temperature at 393K could be as low as 0.058 kJ/m^2, while that at 523K could reach 0.502 kJ/m^2, showing an approximately 9× increase. The fracture toughness of 3D-printed CF/ABS (an amorphous polymeric composite) was 1.2–5.3 kJ/m^2 for non-heated samples and 3.5–5.1 kJ/m^2 for heated samples [1], showing that the heat treatment on the large-scale 3D-printed composites could improve the fracture toughness. However, the effect of adding short carbon fibers on the fracture toughness of large-area 3D-printed amorphous polymer is not yet clear as no comparison was made towards the neat ABS. Further, considering the relatively large size of 3D printed beads (6-10 mm), it is desirable to have a simple fracture test protocol that is based on a single-bead or double-bead configuration rather than a multi-bead system [1, 11].

Here, we propose an experimental method for characterizing mode I fracture toughness of large area additive manufactured (LAAM) short fiber c omposites. To this end, both intrabead fracture toughness (based on the fracture test of a single bead with a single notch) and interbead fracture toughness (based on the fracture test of a double-bead system for evaluating both in-plane and out-of-plane interbead crack propagation) are calculated. The proposed fracture test protocol is expected to be useful for minimizing the amount of materials, and thus speeding up the material selection process since the test can be performed at the bead level. Nonetheless, as the bead-level specimen is rather delicate, bead samples are bonded to the rigid doublers to avoid premature compressive failure at the crack tip. To avoid well-known accuracies caused by doublers when mea-suring fracture toughness [12], we provide a modified data reduction technique based

on Ref. [12] that enables the elimination of the 'doubler effect' in the fracture toughness calculation. Based on the method developed here, we compared the intrabead and interbead fracture toughness of ABS and CF/ABS.

Methods

Materials and additive manufacturing process

Short carbon fiber reinforced acrylonitrile butadiene styrene (CF/ABS) and neat ABS pellets purchased from PolyOne (Avient, Avon Lake, OH, USA) were used as feedstock materials in Baylor University's custom-built large area additive manufacturing (LAAM), having a printe volume of 48" × 48" × 6" [13]. The short fiber content in CF/ABS was set at 13 wt.%. The pellets were dried in a convection oven at 80 °C for 12 hours before the LAAM 3D printing process. As shown in Figure 1a, the pellets were fed into an extruder (Strangpress Model 19, Strangpress, Youngstown, OH, USA) with the following print parameters: nozzle temperature of 220 °C, screw speed of 90 rpm, nozzle flow rate of 9.8 lb/h, nozzle translation speed of 240 cm/min, nozzle diameter of 3.17 mm, and nozzle height above the table of 1.2 mm. Figure 1b shows the 3D printing of CF/ABS from the nozzle. The initial crack of the fracture test specimens was made by inserting a PTFE film between beads during the printing process (see Figure 1c).

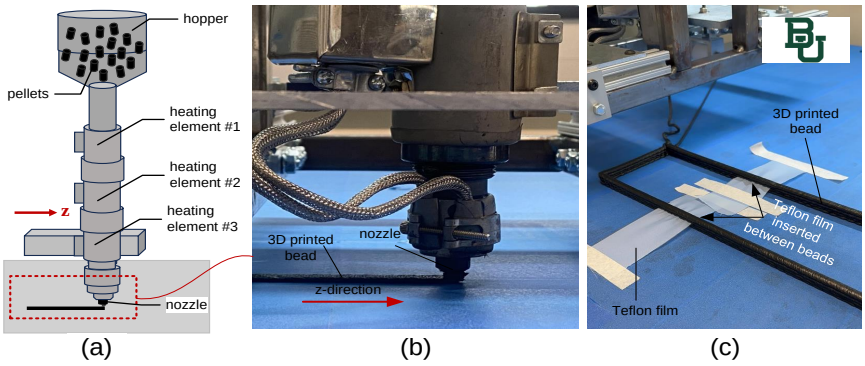

Figure 1: 3D printing process using large area additive manufacturing machine: (a) schematic representation of extrusion process, (b) actual extrusion process, (c) insertion of Teflon film between beads to create an initial crack.

Test specimens and fracture test protocols

The schematics of test specimens used to evaluate the intrabead and interbead fracture toughness are shown in Figure 4 (top row). The nominal dimensions of the individual bead are 8 mm wide and 2.5 mm thick. A preliminary test was performed to

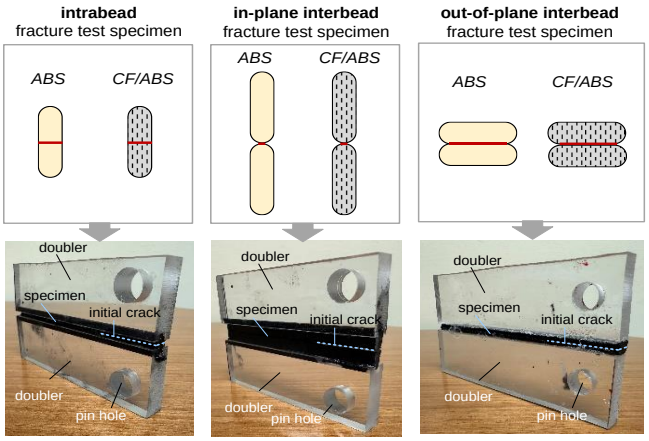

Figure 2: Mode I fracture test configurations (intrabead, in-plane interbead, out-of-plane interbead) and the fracture test specimens with doublers.

ensure good bonding between the individual bead and loading blocks/hinges (according to ASTM D5528 [14]), and to prevent a premature compressive failure causing a discrepancy in the fracture toughness calculation (based on the usual beam theory or compliance calibration). However, the preliminary testing showed that loading blocks or hinges produced compressive failure at the crack tip, disabling the observation of crack crack growth. Thus, doublers made of acrylic were manufactured. Three configurations for measuring mode I fracture of single-bead and double-bead systems are shown in Figure 2 (bottom row). A single-bead system was used to measure intrabead fracture toughness, while a double-bead system measured in-plane and out-of-plane interbead fracture toughness. The rigid doublers were bonded to the specimen using structural adhesive (Scotchweld DP8005). A preliminary test showed that the doublers could prevent a premature failure at the crack tip, allowing the crack propagation.

Mode I fracture was performed using a universal test machine (TestResources Model 100-1000-6, TestResources Inc., Shakopee, MN) with a load cell capacity of 4.4 kN (1000 lbf). A simple fixture was made to connect the loading pins (that were inserted into the doublers) with the gripping system. A displacement-control loading was applied to the specimen at 1 mm/min, while the crack length was recorded using a handheld microscope system (Dino-Lite Edge, Microscope LLC, Roanoke, VA). An example of crack propagation observed during the fracture test using interbead specimen is shown in Figure 3 where the crack shown has propagated from the tip with an initial crack length of a_0 to a of approximately 38 mm.

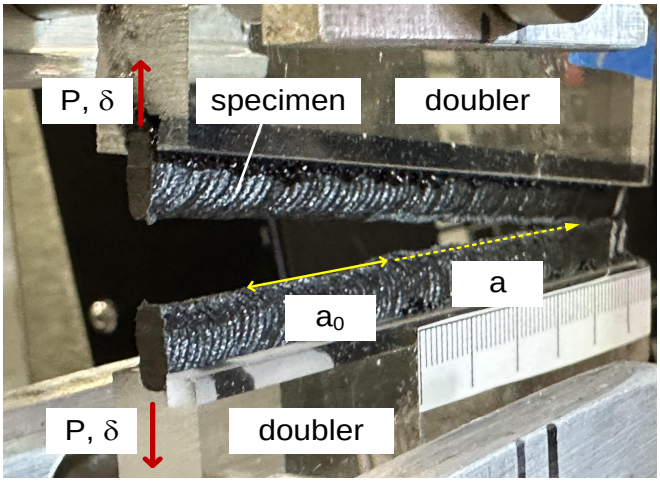

Figure 3: Crack propagation during fracture test of in-plane interbead specimen configuration. Upon mode I loading (opening), the crack propagates from initial crack length a_0 to crack at length a.

Data reduction techniques

The data reduction technique to calculate the strain energy release rate in mode I (G_{IC}) of specimens with bonded doublers was derived based on the proposed method by Reeder et al. [12]. One modification was made to the original method by introducing a varying specimen width. The width of the specimen was not necessarily the same as that of the doublers, and this affected the total second moment of inertia (I). First, the strain energy release rate is given

$$G_{Ic} = \frac{P^2}{2b}\frac{\partial C}{\partial a} \tag{1}$$

where P is the load, b is the specimen width, C is the compliance (deflection/load, δ/P), and a is the crack length. We employed the Euler-Bernoulli beam theory to estimate the arm deflection (δ) due to the point load at one end. We can express the first derivation of compliance C as a function of a

$$\frac{\partial C}{\partial a} = \frac{2a^2}{EI} \tag{2}$$

By substituting Eq. 2 into Eq. 1, we obtain the strain energy release rate in mode I:

$$G_{Ic} = \frac{P^2 a^2}{bEI} \tag{3}$$

The effect of bonded doublers on Eq. 3 was made by introducing a corrected flexural modulus (EI). Here, EI must be replaced with the total flexural modulus consisting of the flexural moduli of the doubler E_d and specimen E_s, as well as the second moment of inertia of the doubler I_d and specimen I_s as follows:

$$EI = E_d(I_d + A_d|\bar{z}_d - \bar{z}|^2) + E_s(I_s + A_s|\bar{z}_s - \bar{z}|^2) \tag{4}$$

where A_d and A_s are the cross-sectional area of the doubler and sample, respectively; $\bar{z}_d$ and $\bar{z}_s$ are the local distance from the neutral axis of the doubler and sample, respectively; $\bar{z}$ is the distance measured from the global neutral axis. The schematic cross-section of the fracture test specimens is given in Fig. 4. The elastic modulus of rigid doubler E_d (acrylic plastic) was 3 GPa. E_s of ABS and CF/ABS obtained from tensile tests were 2.22 GPa and 2.56 GPa, respectively [15]. The second moment of inertia of the doubler and specimen is, respectively, given

$$I_d = \frac{b_d h_d^3}{12} \tag{5}$$

$$I_s = \frac{b_f h_s^3}{12} \tag{6}$$

where all dimensions are defined in Fig. 4. The cross-sectional area of the doubler and sample is given

$$A_d = b_d h_d \tag{7}$$

$$A_s = b_f h_s \tag{8}$$

The local distance from the neutral axis of the doubler and sample is given

$$\bar{z}_d = h_s + \frac{h_d}{2} \tag{9}$$

$$\bar{z}_s = \frac{h_s}{2} \tag{10}$$

The distance measured from the global neutral axis $\bar{z}$ is given

$$\bar{z} = \frac{(E_d/E_s)A_d\bar{z}_d + A_i\bar{z}_i}{(E_d/E_s)A_d + A_i} \tag{11}$$

X-ray micro-computed tomography

X-ray micro-computed tomography (XCT) was employed to identify the interfacial condition between beads before testing. The NSI X3000 X-ray system (North Star Imaging, Rogers, MN, USA) was used to scan the specimen. The X-ray source was set at a voltage of 60 kV, current of 900 μA, and resolution (voxel size) of 15 μm.

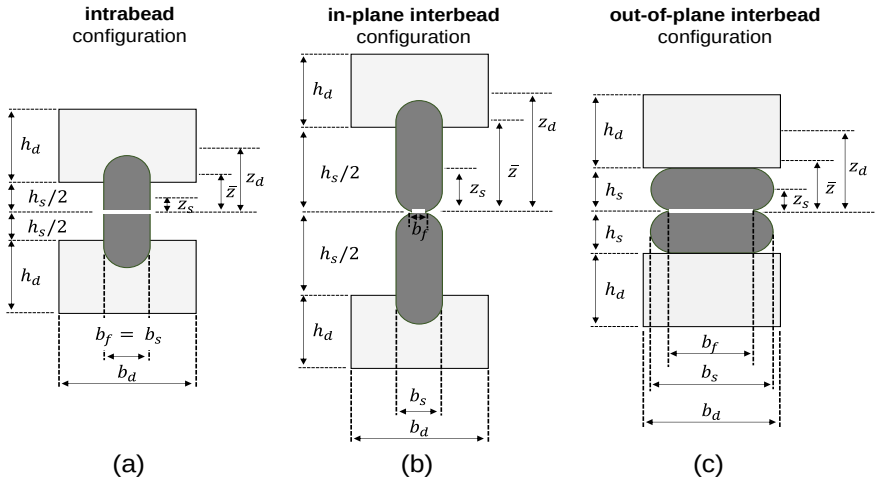

Figure 4: Geometrical information of the fracture test specimens: (a) intralayer, (b) interlayer, in-plane, (c) interlayer, out-of-plane.

The sample was rotated 360 degrees with 1-degree increments to provide volumetric information related to each sample. The scan data was then reconstructed using efX-CT software (North Star Imaging, Rogers, MN, USA). An outlier median filter was used to reduce the scan noise during the reconstruction step. The reconstructed data was subsequently imported into VGStudio Max 3.4 software (Volume Graphics GmbH, Heidelberg, Germany). The VGDefX Porosity Analysis Module, integrated within the VGStudio Max [16], was specifically employed for void identification.

Results and discussion

Figure 5a-f shows the recorded global mechanical response of specimens tested at different fracture configurations, represented by the force-displacement curves. Note that the attained peak load (P_{max}) of the specimens still includes the effect of rigid doublers, which may overestimate the actual peak load of the specimen without doublers. Nonetheless, Figure 5 generally shows that neat ABS outperformed CF/ABS in terms of P_{max}, indicating that the crack is more difficult to initiate in the ABS compared to CF/ABS.

The magnitude of averaged P_{max} for each group is shown in Figure 5a-f. The degradation of force after P_{max} corresponds to crack propagation within the bead (in the case of intrabead fracture) or at the interface between beads (in the case of interbead fracture). The gradual force 'decay' is seen for ABS specimens tested in intrabead (Figure 5a), in-plane interbead (Figure 5b), and CF/ABS specimens tested in in-plane interbead (Figure 5d and f). Alternatively, the abrupt load drop was displayed by ABS specimens

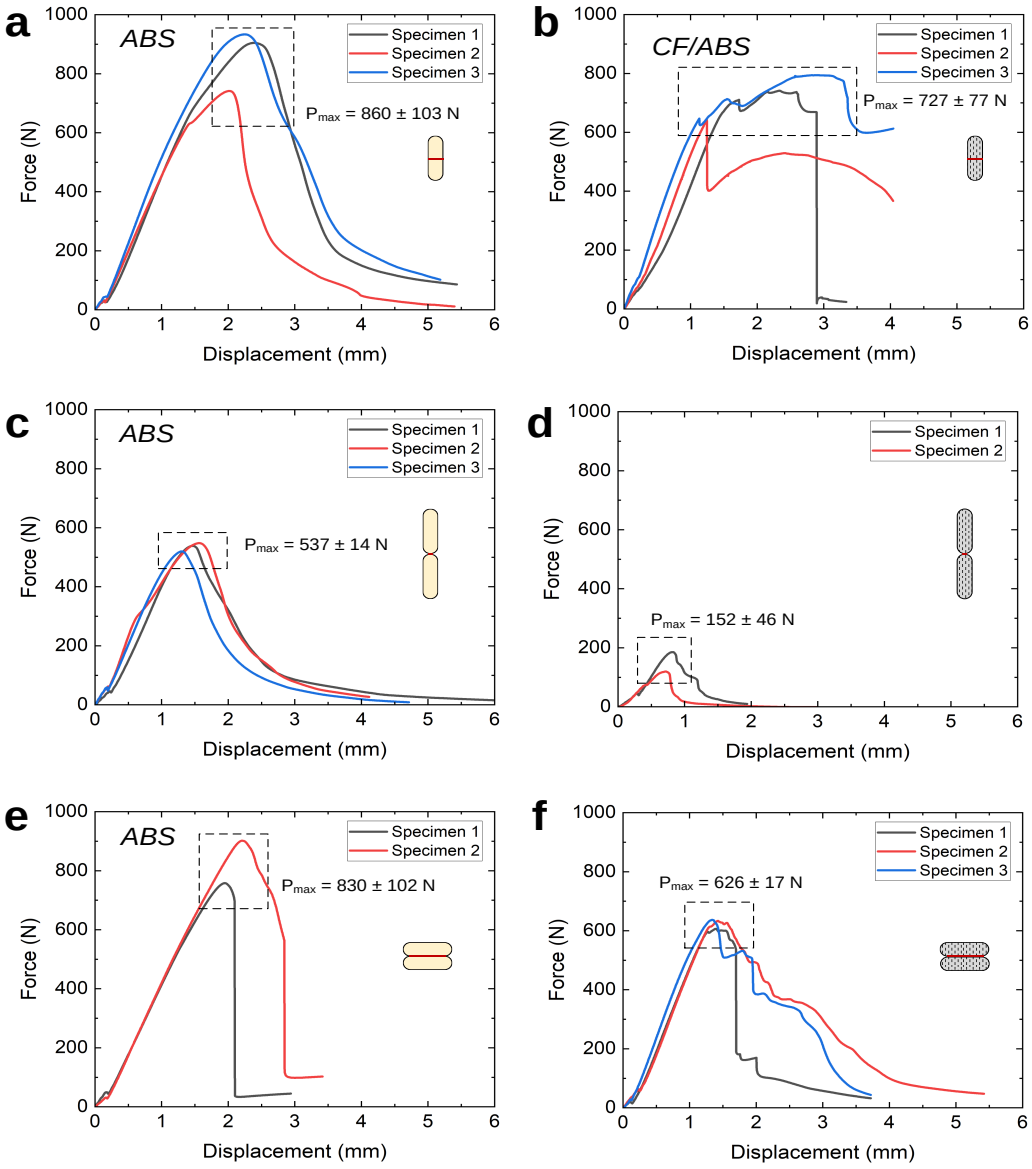

Figure 5: Load-displacement curves obtained from mode I fracture test: (a) intrabead, ABS, (b) intrabead, CF/ABS, (c) in-plane interbead, ABS, (d) in-plane interbead, CF/ABS, (e) out-of-plane interbead, ABS, (f) out-of-plane interbead, CF/ABS.

tested in out-of-plane interbead (Figure 5e), and CF/ABS specimens tested in intrabead (Figure 5b) and out-of-plane interbead (Figure 5f). Here, gradual decay and abrupt

load drop indicate stable and unstable crack propagation, respectively. The specimen with higher P_{max}, as shown in Figure 5, suggests that its fracture toughness G_{Ic} (in both initiation and propagation) is higher than that with lower P_{max} (see again Eq. 3).

Fig. 6 compares G_{Ic} between neat ABS and CF/ABS obtained from three test configurations. Table 1 summarizes G_{Ic} computed with Eq. 3 for all tested specimens. Intrabead fracture toughness of ABS is 75% higher than that of CF/ABS. Interbead fracture toughness in the in-plane direction of ABS is 15× than that of CF/ABS, while the interbead fracture toughness in the out-of-plane direction of ABS is approximately 3.4× than that of CF/ABS. One of the factors contributing to the crack propagation, at least at the interface between beads, is the fact that voids were found at the interface. As shown in Figure 7, the interface at the interbead of CF/ABS consists of aligned fibers and a relatively high volume fraction of voids of nearly 16%. Voids in composites are known as the crack initiator and crack-path provider, contributing to unstable crack growth and lower fracture toughness value.

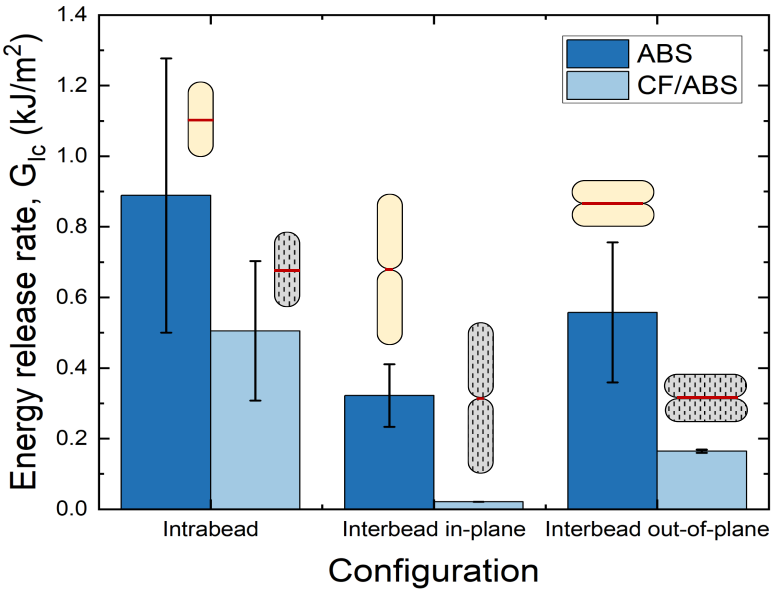

Figure 6: Comparison of 'pure' strain energy release rate between ABS and CF/ABS obtained from three single-bead test configurations.

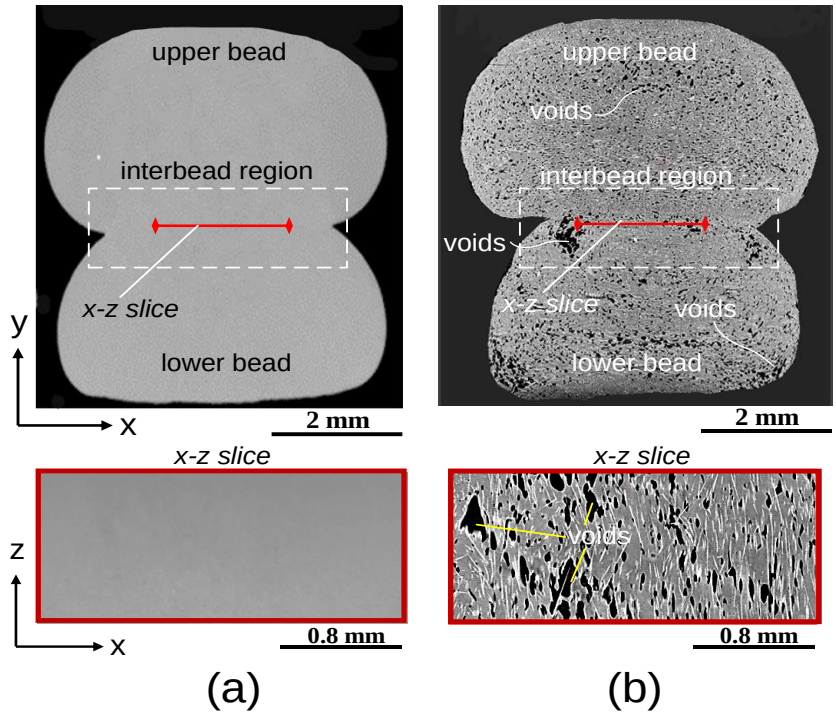

Figure 7: X-ray computed tomography of beads and inter-bead region in (a) ABS, (b) CF/ABS.

Table 1: Fracture toughness at initiation G_{Ic} (in kJ/m^2) of ABS and CF/ABS specimens.

Fracture direction	ABS	CF/ABS
Intrabead	0.89 ± 0.39	0.51 ± 0.20
Interbead, in-plane	0.32 ± 0.09	0.02 ± 0.00
Interbead, out-of-plane	0.56 ± 0.20	0.17 ± 0.01

Concluding remarks and prospective

The fracture test protocol using single- and double-bead systems for measuring intrabead and interbead fracture toughness of 3D-printed large-area short carbon fiber-reinforced ABS composites is presented. The data reduction method for removing the influence of rigid doublers used to connect the specimen and the fixture of the double cantilever beam is also provided. We found that the short carbon fibers generally reduce the fracture toughness of ABS by more than 40%, indicating that the fracture behavior of ABS is modified by the presence of short carbon fibers even at a fiber volume fraction of 18%. Further, the interbead fracture toughness was measured in the in-

plane direction of 3D-printed ABS at 0.32 kJ/m^2, while that of CF/ABS at 0.02 kJ/m^2. Micro-computed tomography analysis revealed that voids between two CF/ABS beads are likely responsible for initiating and speeding up crack propagation, causing a lower resistance-to-fracture of the CF/ABS. In the future, we will compare the fracture test results of ABS and CF/ABS using the present single- or double-bead systems with that of the multi-bead systems. We will also study the influence of cross-bead direction and mechanical post-processing on the fracture toughness of ABS and CF/ABS.

References

[1] V. Kishore, C. Ajinjeru, A. Nycz, B. Post, J. Lindahl, V. Kunc, C. Duty, Infrared preheating to improve interlayer strength of big area additive manufacturing (baam) components, Additive Manufacturing 14 (2017) 7–12.

[2] A. Awenlimobor, D. Smith, Z. Wang, Investigating the effect of generalized newtonian fluid on the micro-void development within large scale polymer composite deposition beads, in: 34th Solid Freeform Fabrication, 2023.

[3] A. Awenlimobor, D. E. Smith, Z. Wang, Simulation of fiber-induced melt pressure fluctuations within large scale polymer composite deposition beads, Additive Manufacturing 80 (2024) 103980.

[4] R. J. Rodriguez JF, Thomas JP, Maximizing the strength of fused-deposition abs plastic parts, in: 10th Solid Freeform Fabrication, Austin, TX, 1999.

[5] K. R. Hart, E. D. Wetzel, Fracture behavior of additively manufactured acrylonitrile butadiene styrene (abs) materials, Engineering Fracture Mechanics 177 (2017) 1–13.

[6] P. Rezaeian, M. R. Ayatollahi, A. Nabavi-Kivi, N. Razavi, Effect of printing speed on tensile and fracture behavior of abs specimens produced by fused deposition modeling, Engineering Fracture Mechanics 266 (2022) 108393.

[7] C. R. Bernal, P. M. Frontini, R. Herrera, Fracture toughness determination of abs polymers using the j-method, Polymer Testing 11 (4) (1992) 271–288.

[8] C. R. Bernal, A. N. Cassanelli, P. M. Frontini, A simple method for j-r curve determination in abs polymers, Polymer Testing 14 (1) (1995) 85–96.

[9] M. Lu, C. Lee, F. Chang, Fracture toughness of acrylonitrile-butadiene-styrene by j-integral methods, Polymer Engineering & Science 35 (18) (1995) 1433–1439.

[10] I. Narisawa, M. Takemori, Fracture toughness of impact-modified polymers based on the j-integral, Polymer Engineering & Science 29 (10) (1989) 671 – 678.

[11] E. Barocio, B. Brenken, A. Favaloro, R. B. Pipes., Interlayer fusion bonding of semi-crystalline polymer composites in extrusion deposition additive manufacturing, Composites Science and Technology 230 (2022) 109334, recent Advances in Composites Science Technology – A special issue in memoriam Prof. Dr.-Ing. Dr. h.c. mult. Klaus Friedrich.

[12] J. R. Reeder, K. Demarco, K. S. Whitley, The use of doubler reinforcement in delamination toughness testing, Composites Part A: Applied Science and Manufacturing 35 (11) (2004) 1337–1344.
[13] N. Sayah, D. E. Smith, Effect of process parameters on void distribution, volume fraction, and sphericity within the bead microstructure of large-area additive manufacturing polymer composites, Polymers 14 (23) (2022).
[14] Standard test method for mode i interlaminar fracture toughness of unidirectional fiber-reinforced polymer matrix composites, ASTM International (2022).
[15] T. D. Russel, Mechanical and thermal property prediction in single beads of large area additive manufactured short-fiber polymer composites, Ph.D. thesis, Baylor University (2021).
[16] G. Stano, N. Sayah, D. E. Smith, T. J. Fleck, Effect of process parameters in additively manufactured sensors prepared via material extrusion processes: Correlation among electrical, mechanical and microstructure properties, Additive Manufacturing Letters 9 (2024) 100194.